analytical chemistry

Subscriber access provided by UNIVERSITY OF BRIGHTON

Article

Novel Single-Enzyme Assisted Dual Recycle Amplification Strategy for Sensitive Photoelectrochemical MicroRNA Assay

Lingying Xia, Mengjie Li, Haijun Wang, Ruo Yuan, and Ya-qin Chai

Anal. Chem., **Just Accepted Manuscript** • DOI: 10.1021/acs.analchem.0c02752 • Publication Date (Web): 27 Sep 2020

Downloaded from pubs.acs.org on September 27, 2020

Just Accepted

"Just Accepted" manuscripts have been peer-reviewed and accepted for publication. They are posted online prior to technical editing, formatting for publication and author proofing. The American Chemical Society provides "Just Accepted" as a service to the research community to expedite the dissemination of scientific material as soon as possible after acceptance. "Just Accepted" manuscripts appear in full in PDF format accompanied by an HTML abstract. "Just Accepted" manuscripts have been fully peer reviewed, but should not be considered the official version of record. They are citable by the Digital Object Identifier (DOI®). "Just Accepted" is an optional service offered to authors. Therefore, the "Just Accepted" Web site may not include all articles that will be published in the journal. After a manuscript is technically edited and formatted, it will be removed from the "Just Accepted" Web site and published as an ASAP article. Note that technical editing may introduce minor changes to the manuscript text and/or graphics which could affect content, and all legal disclaimers and ethical guidelines that apply to the journal pertain. ACS cannot be held responsible for errors or consequences arising from the use of information contained in these "Just Accepted" manuscripts.

is published by the American Chemical Society. 1155 Sixteenth Street N.W., Washington, DC 20036

Published by American Chemical Society. Copyright © American Chemical Society. However, no copyright claim is made to original U.S. Government works, or works produced by employees of any Commonwealth realm Crown government in the course of their duties.

Novel Single-Enzyme Assisted Dual Recycle Amplification Strategy for Sensitive Photoelectrochemical MicroRNA Assay

Ling-Ying Xia, Meng-Jie Li, Hai-Jun Wang, Ruo Yuan*, Ya-Qin Chai*

Key Laboratory of Luminescence Analysis and Molecular Sensing (Southwest University), Ministry of Education, College of Chemistry and Chemical Engineering, Southwest University, Chongqing 400715, PR China

* Corresponding author. Tel.: +86-23-68252277; Fax: +86-23-68253172.

E-mail address: yuanruo@swu.edu.cn (R. Yuan); yqchai@swu.edu.cn (Y. Q. Chai)

Abstract:

Herein, a novel single-enzyme assisted dual recycle amplification strategy based on T7 exonuclease (T7 Exo) and strand displacement reaction (SDR) was designed to fabricate photoelectrochemical (PEC) biosensor for sensitive microRNA-141 (miRNA-141) detection with use of laminar bismuth tungstate (Bi_2WO_6) as photoactive material. Compared with traditional enzyme assisted dual recycle amplification strategy, the presented method could effectively refrain enzyme interference reaction, reduce environmental sensitivity and save cost. Here, hairpin DNA1 (H1) decorated on magnetic beads (MB) hybridized with target miRNA-141 to form H1/miRNA-141 heteroduplex. With the introduction of hairpin DNA2 (H2) labeled SiO_2 (H2-SiO_2), SDR was triggered between H2-SiO_2 and H1, thus miRNA-141 was displaced from H1/miRNA-141 heteroduplex and H1/H2-SiO_2 duplex was formed, realizing the reuse of target. In the existence of T7 Exo, the H1/H2-SiO_2 duplex was digested with the release ofoutput DNA-SiO_2. To enhance the target conversion rate, H1-MB was intactly released and cycled, which could initiate more T7 Exo digestion and freed abundant output DNA-SiO_2. Through such a process, a tiny miRNA-141 could induced substantial output DNA-SiO_2, effectively improving the target amplification efficiency and detection sensitivity of PEC biosensor. Furthermore, Bi_2WO_6 was modified on electrode to provide a superior initial PEC signal due to its excellent electronic transformation capacity. With the introduction of output DNA-SiO_2, the hairpin structure of H3 on electrode was opened, making SiO_2 close to the electrode surface,

which significantly decrease the PEC signal. This work firstly established a PEC biosensor featured a single-enzyme assisted dual recycle amplification process for sensitive detection of biomarkers.

Keywords : photoelectrochemical biosensor; single-enzyme assisted dual recycle amplification strategy; laminar Bi_2WO_6; miRNA-141

Introduction:

Enzyme assisted recycle amplification strategy, a powerful biological amplification technique has been widely developed in photoelectrochemical (PEC) biosensor.[1-5] The application of enzyme assisted recycle amplification strategies lay a firm foundation for the improvement of target molecule amplification efficiency and sensitivity of PEC biosensor.[6-8] In the past decades, enzyme assisted single recycle amplification strategies have been mainly developed to achieve the conversion of bits of target to substantial mimic target due to its low cost and easy operation.[9-12] For instance, our group has reported a "signal off" PEC biosensor for microRNA-141 (miRNA-141) assay on the basis of a duplex specific nuclease assisted single recycle procedure.[13] Li and his coworkers has constructed a PEC biosensor using T7 exonuclease (T7 Exo) cleaves the DNA/RNA heteroduplex to release RNA (target) and achieve the target amplification.[14] The target molecule could be effectively amplified in the reported works, nevertheless, the amplification efficiency was still requires further improvement since each input target could only be conversed to one mimic target in once recycle. Low conversion ratio frequently leads to unsatisfactory amplification efficiency and detection sensitivity of PEC biosensor. Therefore, it is meaningful to design an enzyme assisted recycle amplification strategy with a target-to-mimic target conversion ratio of 1:N (N>1), which can enhance the amplification efficiency, further improving sensitivity of PEC biosensor.

With the purpose to increase the target conversion ratio, enzyme-assisted dual

recycle amplification strategies were recently proposed in the construction of PEC biosensor, in which two cycles was initiated with twice enzymatic cleavages, achieving the cascade amplification of target.[15,16] To date, great efforts have been spurred in the construction of enzyme assisted dual recycle amplification strategy. For example, Knopp has studied a dual recycle amplification strategy based on polymerase and Nt.BbvCI (nicking enzyme) for the construction of PEC biosensor.[17] Recently, our group has presented a dual recycle amplification strategy with the assistance of Exo Ⅲ, which was simultaneously used in two cycles.[18] In these constructed methods, target conversion ratio was obviously increased. However, the commonly-applied strategies still suffered from some drawbacks including significantly interferential reaction caused by different enzymatic cleavage process, highly environmental sensitivity and high cost ascribed to the application of different enzymes. Therefore, a single-enzyme assisted dual recycle amplification strategy was proposed to overcome those above problems by combining strand-displacement reaction (SDR)[19-21] and T7 Exo[22-25] to circumvent interferential reaction, decrease environmental sensitivity and save cost. As a result, the proposed single-enzyme assisted dual recycle amplification strategy would provide eminent amplification efficiency and excellent the sensitivity of PEC assay.

In this work, a novel PEC biosensor on the basis of the single-enzyme assisted dual recycle amplification strategy and laminar bismuth tungstate (Bi_2WO_6) as photoactive material was constructed for the detection of miRNA-141. Bi_2WO_6 as a new type photoactive material has been employed in various fields including

photocatalyst for degradation of organic pollutants, carbon dioxide reduction, and water splitting due to its excellent photoelectronic properties.[26-33] In particular, laminar Bi_2WO_6 exhibit more excellent photoelectric conversion efficiency than that of conventional particle Bi_2WO_6 because its unique laminated structure is beneficial to the charge transformation.[34] As depicted in Scheme 1, laminar Bi_2WO_6 was adopted as photoactive material due to its extremely excellent photoelectric properties, which was coated onto bare glass carbon electrode (GCE) to provide a superior initial photocurrent. Then, gold nanoparticles (Au NPs) were deposited on the electrode to provide the immobilization sites of DNA. Followed by hairpin DNA3 (H3) was immobilized on the modified electrode surface by Au-N bond, the blocking agent hexanethiol (HT) was added on the resultant electrode to blocking nonspecific binding sites. Subsequently, the hairpin structure of H3 was opened by the output DNA-SiO_2 generated from the single-enzyme assisted dual recycle amplification process, making SiO_2 close to the electrode surface and leading to an obviously decreased PEC response owing to the steric hindrance effect of SiO_2, accordingly achieving sensitive detection of miRNA-141. The proposed PEC biosensor featured firstly a novel single-enzyme assisted dual recycle amplification strategy for detection of biomarkers.

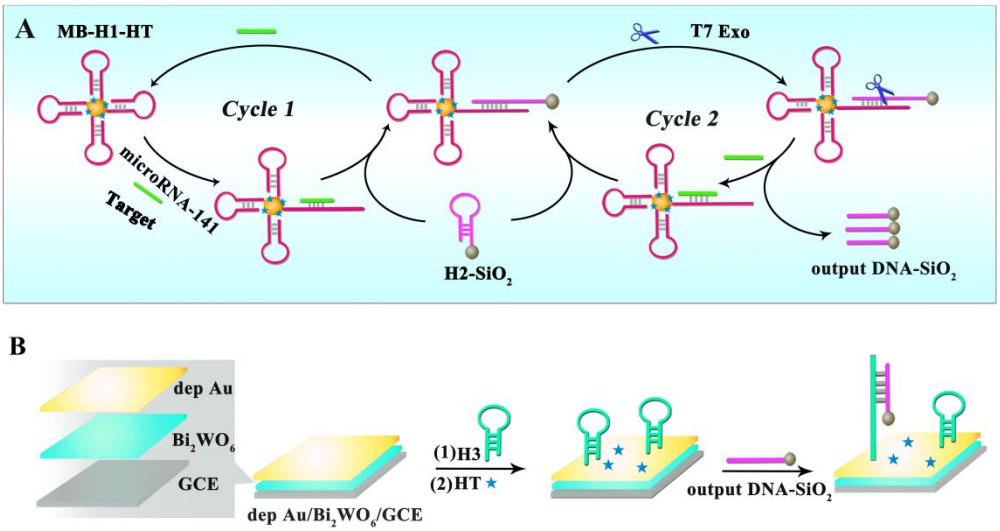

Scheme 1: Schematic diagram of (A) single-enzyme assisted dual recycle amplification process, (B) preparation of the PEC biosensor.

Experimental Section

1. Preparation of Hairpin DNA2 (H2)-SiO_2 NPs Conjugate

The SiO_2 NPs solution was prepared as follows: firstly, 200 μL of tetraethyl orthosilicate, 2 mL of $NH_3 \cdot H_2O$ (28%) and 40 mL of ethanol were added into a beaker and stirring for 2 days, next, the resultant solution was centrifugal washing and re-dispersed in 5 mL ethanol. Then, 35 μL of (3-aminopropyl) triethoxysilane solution (97%) mixed with 4 mL SiO_2 NPs solution and stirring the mixture overnight for obtaining the amino modified SiO_2 NPs (SiO_2-NH_2 NPs). Finally, the SiO_2-NH_2 NPs was washed by ethanol.

The H2-SiO_2 NPs conjugate was synthesized by mixing 10 μL of glutaraldehyde (0.05%), 30 μL of SiO_2-NH_2 NPs, and 1 mL of H2（2.5 μM）stirring the solution for 1 h at room temperature. Finally, the obtained H2-SiO_2 NPs conjugates were centrifugal washing by ethanol and dispersed in 1 mL PBS (pH 7.4) for subsequent application.[35]

2. The Synthesis of Laminar Bi_2WO_6

Laminar Bi_2WO_6 were synthesized by ultrasonication aided hydrothermal process. Firstly, solution A was obtained by dissolving 0.006 M of $Bi(NO_3)_3 \cdot 5H_2O$ into 65 mL of ultrapure water. Next, 0.003 M of $Na_2WO_4 \cdot 2H_2O$ was dissolved into ethylene glycol, which was named as solution B. Subsequently, solution B was dropped into solution A by inches with ultrasonication. The product slurry was blended for 1 h and

hydrothermally reacted in Teflon autoclave at 170 °C for 20 h. The resultant Bi_2WO_6 was repeatedly washed by ethanol and water and lastly dried at 50 °C for overnight.

3. Single-Enzyme Assisted Dual Recycle Amplification Process

Briefly, the target miRNA-141 (10 μL of different concentrations) was added into a solution of magnetic beads (MB)-H1-HT (10 μL). After the H1 on the MB surface hybridized with target miRNA-141 at 37 °C for 0.5 h, the heteroduplex of H1/miRNA-141 was formed. Then, H2-SiO_2 (5 μM, 10 μL) was added and incubated at 37 °C for 2 h, which was able to displace target from H1/miRNA-141 heteroduplex. Thus, the target was reused and H1/H2-SiO_2 duplex was formed. Next, 1 μL of T7 Exo (100 U) was added into the mixture to specially cleave the H1/H2-SiO_2 duplex and incubated for 3 h at 25 °C. As a result, H1-MB-HT and output DNA-SiO_2 were released. Specifically, the released H1 could hybridized with H2-SiO_2, which could bring out substantial output DNA-SiO_2 as mimic target. Followed by gradually cooling the mixture to room temperature, the product was obtained through magnetic separation.

4. Preparation of the Sensing Interface

Followed by ultrasonication before modification in ethanol solution, the bare GCE was preprocessed by alumina powder. Subsequently, the solution of Bi_2WO_6 dissolved in ultrapure water was dropped on the bare GCE surface. Then, the resultant electrode was submerged into 1% of $HAuCl_4$ solution to deposit Au NPs on the surface of modified GCE at -0.2 V for 30 s. Next, H3 (20 μL, 2.5 μM) was incubated on the

modified electrode at 4 °C for 14 h. Lastly, HT (20 μL, 1 mM) was decorated to the electrode surface for blocking nonspecific binding sites. Through such a process, the sensing interface was developed. After every time incubation, the modified electrode was rinsed by ultrapure water to remove needless agents. The PEC biosensor construction process is clearly shown in Scheme 1.

5. The Measurement Method

PEC biosensor measurements were implemented in 7 mL of PBS (pH = 7.0, 0.1 M) with the addition of AA (50 μL, 0.1 M) solution, which was applied as the electron donor. In this measurement system, the excitation light source was light-emitting diode (LED) lamp, and the used excited wavelength was 365 nm with a luminous flux of 31 mW. The test model was set as turned off-on-off for 10-20-10 s at 0.0 V.

Results and Disscussion

1. **Characterization of the Prepared Materials**

The scanning electron microscope (SEM) was employed to characterize the prepared SiO_2 NPs, Au NPs and laminar Bi_2WO_6, which was shown in Figure 1. In Figure 1A, the well-dispersed SiO_2 NPs was clearly observed with average size about 30 nm. The result indicated that the SiO_2 NPs were successfully prepared. In addition, the SEM image of deposited Au NPs on GCE was displayed in Figure 1B. Globular particles in shape could be observed and the diameter was about 200-300 nm. Besides, the prepared laminar Bi_2WO_6 was characterized by SEM under different resolutions, which were shown in Figure 1C to 1E. As can be seen in Figure 1C and 1D, the size of laminar Bi_2WO_6 was about 300 nm with a sheet in shape. In the view of lower resolution than that of Figure 1C, numerous laminar Bi_2WO_6 could be found, which was showed in Figure 1E. Meanwhile, the energy dispersive spectroscopy (EDS) was applied to analyze the elemental mapping of laminar Bi_2WO_6 immobilized onto conductive glass (Indium tin oxide, ITO), the mapping results of Bi, W, O element were exhibited in Figure 1F, 1G and 1H, respectively.

To further verify the successful preparation of laminar Bi_2WO_6, we characterized it by X-ray diffraction (XRD), X-ray photoelectron spectroscopy (XPS) and Raman. XPS was used to analyze elements in laminar Bi_2WO_6, which was shown in Figure 2A. The peaks of Bi 4f, W 4f, and O 1s were detected at 159.4, 35.3, and 530.0 eV,

respectively, which were consistent with reported data and proved the existence of T Bi, W, and O elements.[35-37] In addition, Figure 2A (a-c) displayed the high-resolution Bi 4f, W 4f and O 1s XPS spectra of laminar Bi_2WO_6. In Figure 2B, the Raman analysis of laminar Bi_2WO_6 modified on silicon substrate was performed. The characteristic Raman bands of laminar Bi_2WO_6 located at 305, 713 and 792 cm^{-1} could be observed in Figure 2B (a, c), consisting with the reported literatures. Besides, Figure 2B (b) was the Raman band of silicon substrate. [38-40] Lastly, the crystal structure of laminar Bi_2WO_6 was studied by XRD. As can be seen in Figure 2C, all of the characteristic peaks matched well with the standard data (JCPDS no. 26-1044). From the above results, we could infer that the laminar Bi_2WO_6 were successfully synthesized.

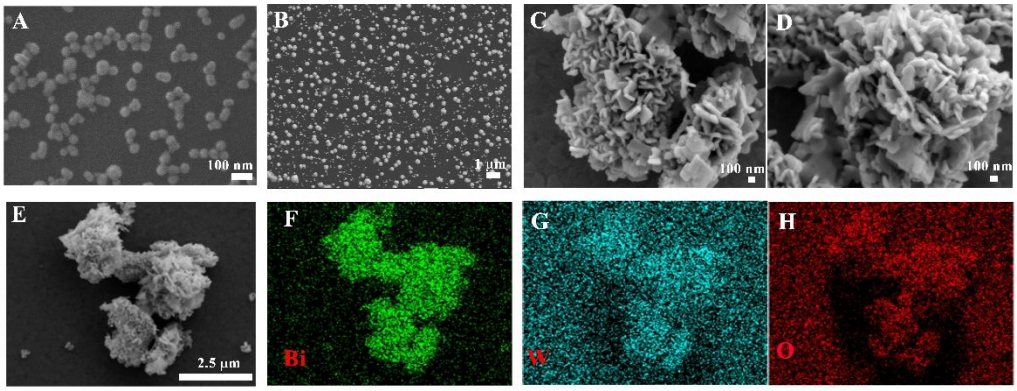

Figure 1 SEM image of (A) SiO_2 NPs; (B) dep Au; (C)-(E) laminar Bi_2WO_6 under different resolutions. (F)-(H) are the corresponding elemental mapping of Bi, W, and O for image E, respectively.

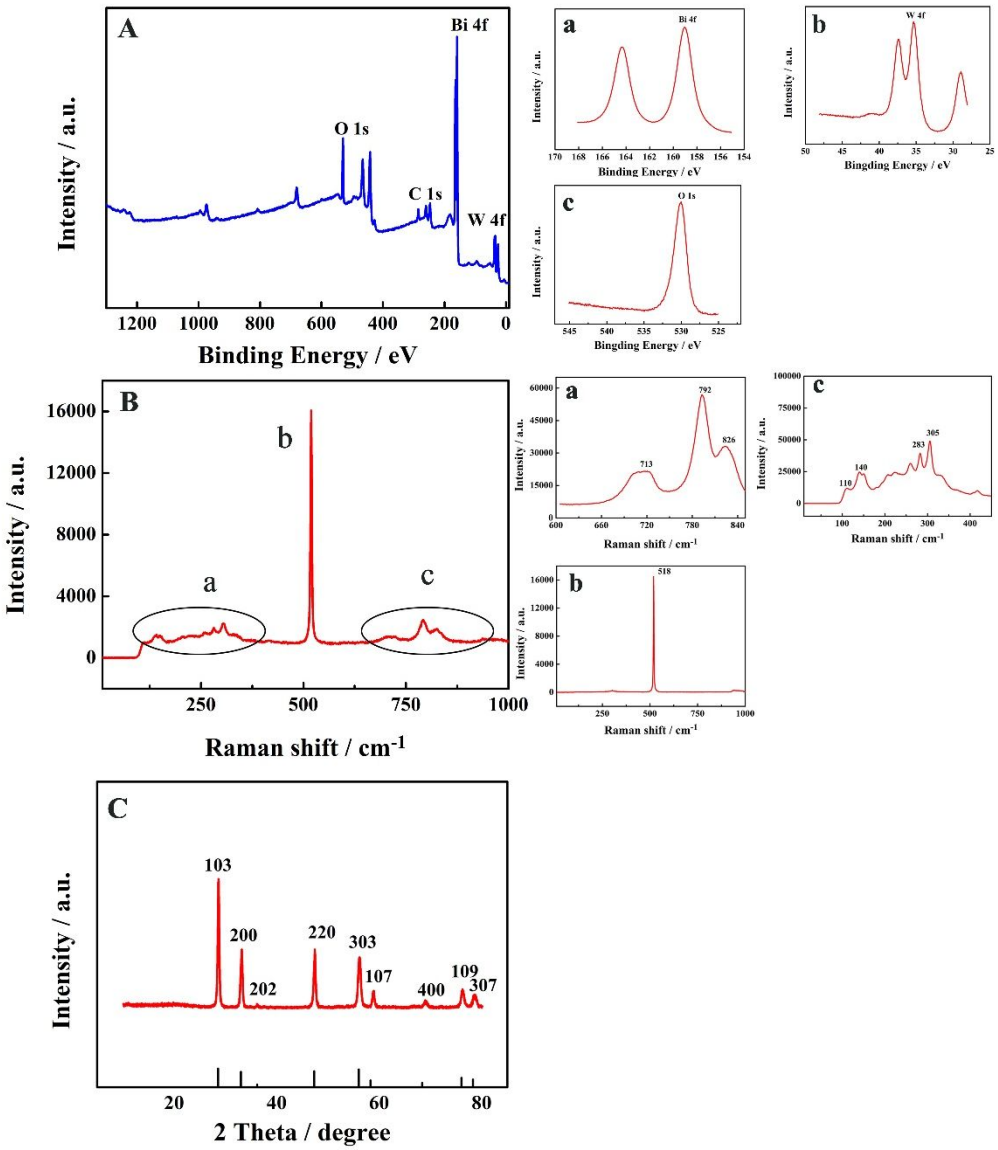

Figure 2. XPS result for (A) the whole region of laminar Bi_2WO_6 (the corresponding image a-c were the Bi 4f region, W 4f region and O 1s region, respectively); (B) Raman study of laminar Bi_2WO_6 (the corresponding image a, c were high resolution in Raman spectra, b was the Raman spectra of the substrate); (C) XRD analysis of laminar Bi_2WO_6.

2. Electrochemical Performance of the Proposed Detection Platform

Cyclic voltammetry (CV) characterization was performed for studying the each step decoration of the proposed detection platform. The corresponding electrode was

immersed into 2 mL of PBS within 5 mM $[Fe(CN)_6]^{3-/4-}$ and 0.1 M KCl at a scan rate of 50 mV/s. As can be seen in Figure 3A, a couple of convertible redox peaks could be observed for the bare GCE (curve a). After the immobilization of Bi_2WO_6 on GCE, the peak current decreased (curve b) caused by the steric-hindrance effect for the electronic transformation. With the deposition of gold nanoparticles (Au NPs) on the resultant electrode surface (dep Au), the current signal of redox peaks evidently increased (curve c), which could be attributed to the outstanding conductivity of Au NPs. After H3 was incubated on the electrode, the H3/Dep Au/GCE showed significantly decreased peak current (curve d) due to the electronic repulsion between the negatively charged H3 and $[Fe(CN)_6]^{3-/4-}$. Next, HT was modified on the resultant GCE to block the nonspecific binding sites, resulting in continued decrease of peak current (curve e). Meanwhile, the construction of PEC sensing interface was characterized with electrochemical impedance spectroscopy (EIS). As can be seen in Figure 3B, in comparison to bare GCE (curve a), the Bi_2WO_6 modified electrode demonstrated a greater charge-transfer resistance (R_{et}) (curve b), indicating that Bi_2WO_6 could hinder the electron transfer. With the Au NPs deposited on the Bi_2WO_6/GCE electrode surface, the value of R_{et} decreased obviously because of the eminent conductivity of Au NPs (curve c). After the stepwise incubating H3 and HT, the R_{et} increased consecutively (curve d and e, respectively) due to the electrostatic repulsion and poor conductivity, respectively. These results manifested that the successful preparation of the PEC biosensor.

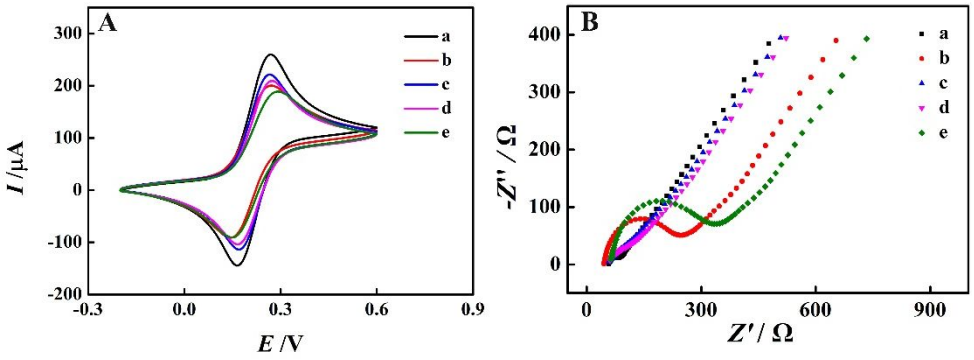

Figure 3 (A) CV profiles and (B) EIS measurement in 0.1 M PBS with 5.0 mM $[Fe(CN)^6]^{3-/4-}$ toward (a) bare GCE; (b) bare GCE (Bi_2WO_6); (c) bare GCE (Au NPs/Bi_2WO_6); (d) bare GCE (H3/Au NPs/Bi_2WO_6); (e) bare GCE (HT/H3/Au NPs/Bi_2WO_6), respectively.

3. PEC Characterization of Biosensing Interface.

For the express purpose of confirming the successful construction of PEC biosensing interface, the PEC characterization of stepwise was conducted. As shown in Figure 4, a near zero PEC signal was observed of the bare GCE (curve a). Then, an obviously enhanced photocurrent was obtained (curve b) with the immobilization of photoactive material Bi_2WO_6, indicating that Bi_2WO_6 could be used as an excellent photoactive material to provide superior initial photocurrent signal for the establishment of PEC biosensor. After Au NPs were deposited on the modified electrode surface, the PEC signal was evidently enhanced (curve c). With the incubation of DNA H3 on resultant electrode surface, the photocurrent reduced due to the poor conductivity of DNA strand (curve d). As expected, a further decreased photocurrent could be detected (curve e) with the modification of HT, which was used as blocking agent to blocking nonspecific sites. With the decoration of output DNA-SiO_2, the PEC signal was obviously decreased (curve f) derived from the steric-hindrance effect of

SiO_2. The results demonstrated that the preparation of the PEC biosensing interface was successful.

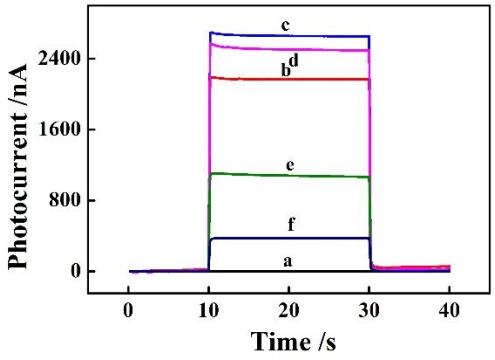

Figure 4. PEC responses of (a) bare GCE; (b) bare GCE (Bi_2WO_6); (c) bare GCE (Au NPs/Bi_2WO_6); (d) bare GCE (H3/Au NPs/Bi_2WO_6); (e) bare GCE (HT/H3/Au NPs/Bi_2WO_6); (f) bare GCE(output DNA-SiO_2/ HT/H3/Au NPs/Bi_2WO_6).

4. Characterization of the Fabrication Process of Sensing Interface

The SEM and EDS-mapping characterization results were shown in Figure 3. Figure 3A showed the image of laminar Bi_2WO_6 immobilized on bare GCE and the sheet in shape of Bi_2WO_6 was widely dispersed on the surface of GCE, which demonstrated Bi_2WO_6 was successfully modified on GCE. Large amounts of Au NPs could be observed after Au NPs were deposited on the electrode surface (Figure 3B). Meanwhile, the step for deposition of Au NPs onto Bi_2WO_6/GCE was characterized by EDS-mapping, as expected, Au, Bi, W and O elements were obviously presented in Figure 3C-3F, respectively. Subsequently, Figure 3G and 3H showed the SEM images of H3 incubated on the resulted dep Au/ Bi_2WO_6/GCE surface under different resolutions. After the incubation of H3, distinct changes of Au NPs could be observed. Besides, the

elements analysis of H3 immobilized on Au NPs surface was shown in Figure 3I and the insert table in I was showed the elemental content for the cycled part of H. The presence of P element proves that H3 was successfully modified onto dep Au/Bi_2WO_6/GCE.

To further investigate the preparation process of the sensing interface, (atomic force microscope) AFM was utilized to characterize the prepared biosensing interface step by step. As seen in Figure 4A, sliced structure of laminar Bi_2WO_6/GCE could be clearly observed, indicating that laminar Bi_2WO_6 was successfully modified on GCE. In Figure 4B, obvious particle Au on laminar Bi_2WO_6 was found after the deposition of Au NPs on Bi_2WO_6/GCE. Lastly, obvious changes on the AFM image of H3/dep Au/ Bi_2WO_6/GCE could be observed compared with the AFM image of dep Au/ Bi_2WO_6/GCE, which proved that H3 was successfully modified to dep Au/ Bi_2WO_6/GCE. The above characterization results indicate that our sensor construction process is successful.

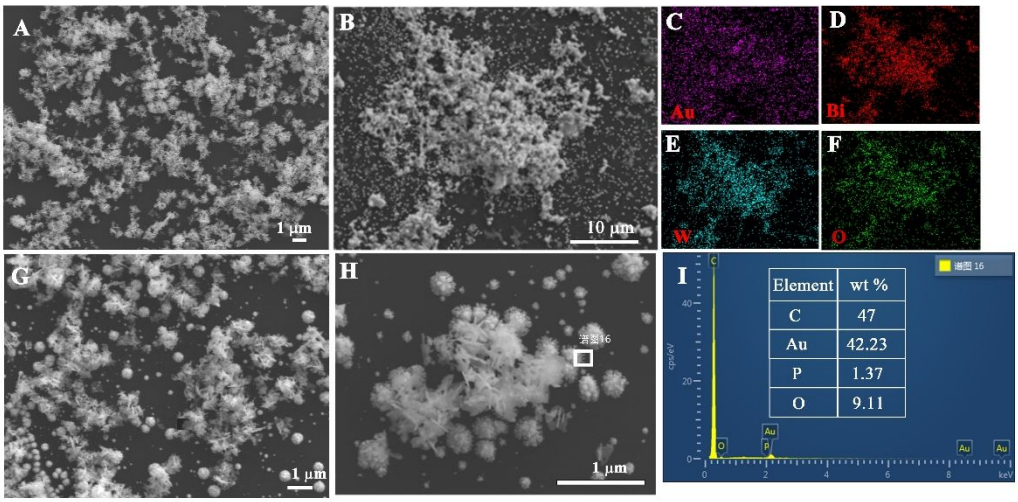

Figure 5. SEM images of the immobilized of (A) laminar Bi_2WO_6 on GCE, (B) dep Au/laminar Bi_2WO_6 on GCE, (G) H3/dep Au/laminar Bi_2WO_6 on GCE. (C)-(F) the elemental mapping of Au, Bi, W and O, respectively. (H) The sampling region of EDS analysis of H3/dep Au/laminar Bi_2WO_6/GCE and (I) the corresponding EDS analysis for the cycled part in H (the insert table in I showed the elemental content for the cycled part in H).

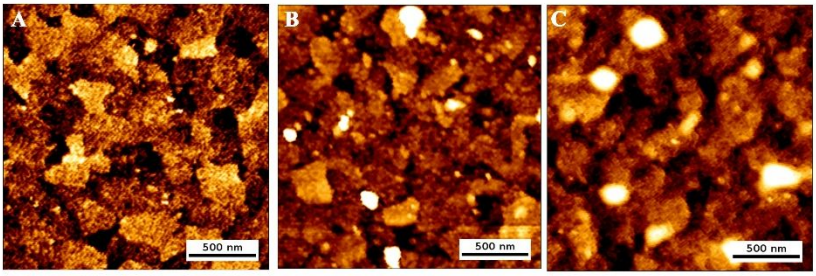

Figure 6. AFM images of the immobilized of (A) laminar Bi_2WO_6 on GCE, (B) dep Au/laminar Bi_2WO_6 on GCE, (C) H3/dep Au/laminar Bi_2WO_6 on GCE.

5. PEC Performance of the Proposed Platform

To evaluate the analytical performance of the presented PEC biosensing platform, the photocurrent signal was measured toward a serious of miRNA-141concentrations with the optimal conditions, which was exhibited in Figure 7A. The photocurrent signal decreased gradually with the increase of miRNA-141 concentration within the range of 0.25 fM ~ 2.5 nM. Figure 7B showed the linear response curve. And the equation of linear regression was I = -117.26 lgc_{target} + 800.79, r = 0.9932, in which r, I and c, respectively, were the correlation coefficient, the photocurrent signal and the concentration of miRNA-141. Besides, based on the expression of $3\sigma/S$ (S and σ were defined as the slope of the fitting curve at low concentrations and the standard deviation of the blank, respectively), 83 aM of limits of detection (LOD) could be obtained.

Meanwhile, the assay performance of the presented detection platform were compared with other reported methods, which was shown in Table 1. It is observed in the results that the presented biosensing platform performed a prominent analytical performance for miRNA-141detection.

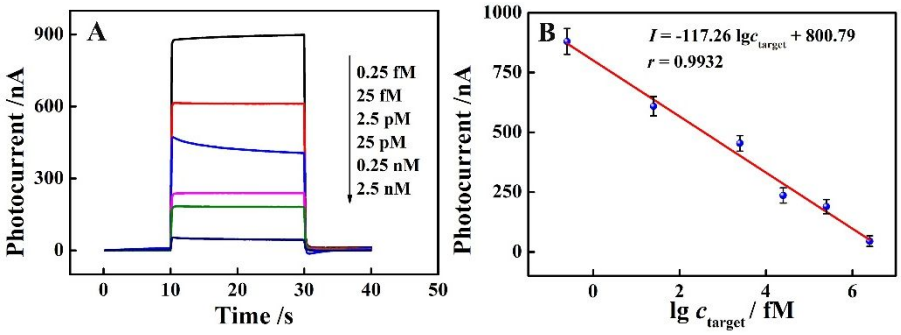

Figure 7. (A) PEC response signals of the constructed PEC biosensor based on single-enzyme dual recycle amplification strategy toward different concentrations of miRNA-141. (0.25 fM ~ 2.5 nM). (B) The linear response curve of the lgc_{target} and PEC response.

Table 1 Comparison of the Reported Works with Our Proposed Method for Detection of miRNA.

analytical method	detection range	limit of detection	references
electrochemistry	5 fM ~ 5 pM	1.92 fM	41
fluorescent	1 pM ~ 2.5 nM	0.21 pM	42
fluorescent	25 pM ~ 10 nM	16.5 pM	43
ECL	0.5 fM ~ 100. pM	0.1 fM	44
PEC	1 fM ~ 1 pM	0.23 fM	45
PEC	1 fM ~ 10 pM	0.5 fM	46

PEC	0.25 fM ~ 2.5 nM	83 aM	***this work***

Abbreviation: ECL = electrochemiluminescence.

6. Specificity and Stability Studies of the Presented Detection Platform.

To study the detection specificity of the designed strategy toward miRNA-141, let-7a, miRNA-21, miRNA-155 and miRNA-182-5p were employed as the interferents and miRNA-141 as target. From Figure 8A, with the incubation of 0.25 nM interferents, strong photocurrent signals were obtained. However, a low PEC signal was recorded in the existence of 2.5 pM miRNA-141. The result demonstrated a preeminent selectivity of the constructed detection platform. Furthermore, the PEC biosensor stability was also explored by recording the photocurrent signal toward 25 fM of miRNA-141 under consecutive 10 cycles with "off-on-off" light illumination at "10-20-10s". Approximate stable photocurrent could be found in Figure 8B and the calculated relative standard deviation (RSD) of 1.0% was obtained, indicating that the proposed strategy possess a satisfied stability.

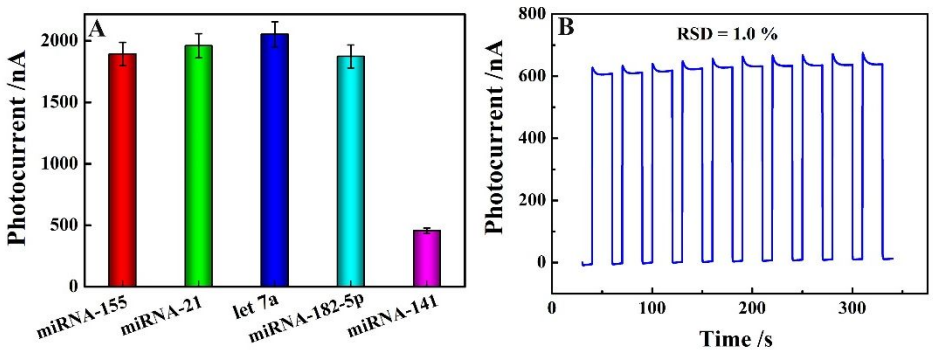

Figure 8. (A) The photocurrent signals of the PEC biosensor incubated with target (2.5 pM) and various interferences (0.25 nM); and (B) the PEC signal of the prepared PEC detection platform

with continuous 10 cycles incubated 25 fM miRNA-141.

4. Conclusion

In conclusion, a new PEC biosensor was prepared based on single-enzyme assisted dual recycle amplification strategy and Bi_2WO_6 as photoactive material for miRNA-141 detection. Herein, the amplification efficiency of target was greatly enhanced attributed to dual recycle of target and substrate in designed single-enzyme assisted dual recycle amplification strategy. Moreover, the application of single enzyme could effectively avoid enzyme interference reaction, decrease the environment sensitivity and save cost, opening a neo-path for improving the sensitivity and accuracy of PEC biosensor. Impressively, the constructed PEC biosensor displayed a wide linear range, high sensitivity, distingushed specificity and stability based on single-enzyme assisted dual recycle amplification strategy, which provides new way for early diagnosis of cancer.

ASSOCIATED CONTENT

Supporting Information. Reagents and apparatus; instruments; the preparation of magnetic beads (MB)-H1-HT conjugate; optimization of the concentration of laminar Bi_2WO_6; mechanism of the electron transformation; PAGE analysis and characterization of H2-SiO_2 NPs and MB-H1-HT conjugates. The Supporting Information is available free of charge on the ACS Publications website.

AUTHOR INFORMATION

Corresponding authors:

Ruo Yuan - Key Laboratory of Luminescence Analysis and Molecular Sensing (Southwest University), Ministry of Education, College of Chemistry and Chemical Engineering, Southwest University, Chongqing 400715, PR China; Phone: +86-23-68252277; Fax: +86-23-68253172; E-mail: yuanruo@swu.edu.cn (R. Yuan)

Ya-Qin Chai - Key Laboratory of Luminescence Analysis and Molecular Sensing (Southwest University), Ministry of Education, College of Chemistry and Chemical Engineering, Southwest University, Chongqing 400715, PR China; Phone: +86-23-68252277; Fax: +86-23-68253172; E-mail: yqchai@swu.edu.cn (Y. Q. Chai)

Authors

Ling-Ying Xia - Key Laboratory of Luminescence Analysis and Molecular Sensing (Southwest University), Ministry of Education, College of Chemistry and Chemical Engineering, Southwest University, Chongqing 400715, PR China;

Meng-Jie Li - Key Laboratory of Luminescence Analysis and Molecular Sensing (Southwest University), Ministry of Education, College of Chemistry and Chemical Engineering, Southwest University, Chongqing 400715, PR China;

Hai-Jun Wang - Key Laboratory of Luminescence Analysis and Molecular Sensing (Southwest University), Ministry of Education, College of Chemistry and Chemical Engineering, Southwest University, Chongqing 400715, PR China.

ACKNOWLEDGMENTS

This work was financially supported by the National Natural Science Foundation of China (21974108, 21675129, and 21775124) and the Fundamental Research Funds for the Central Universities (XDJK2020TY002), China.

Conflicts of interest

There are no conflicts to declare.

References

1. Yang, H. M.; Hu, M. S.; Li, Z. L.; Zhao, P. N.; Xie, L.; Song, X. R.; Yu, J. H. Donor/Acceptor-Induced Ratiometric Photoelectrochemical Paper Analytical Device with a Hollow Double-Hydrophilic-Walls Channel for microRNA Quantification *Anal. Chem.* 2019, *91*, 14577-14585.

2. Li, M. J.; Tian, X.; Liang, W. B.; Yuan, R.; Chai Y. Q. Ultrasensitive Photoelectrochemical Assay with PTB7-Th/CdTe Quantum Dots Sensitized Structure as Signal Tag and Benzo-4-chlorohexadienone Precipitate as Efficient Quencher *Anal. Chem.* 2018, *90*, 14521-14526.

3. Deng, H. M.; Huang, L. J.; Chai, Y. Q.; Yuan, R.; Yuan, Y. L. Ultrasensitive Photoelectrochemical Detection of Multiple Metal Ions Based on Wavelength-Resolved Dual-Signal Output Triggered by Click Reaction *Anal. Chem.* 2019, *91*, 2861-2868.

4. Gao, X. S.; Cai, Q. Q.; Li, H. K.; Jie, G. F. Supersandwich Nanowire/Quantum

Dots Sensitization Structure-Based Photoelectrochemical "Signal-On" Platform for Ultrasensitive Detection of Thrombin *Anal. Chem.* 2020, *92*, 6734-6740.

5. Li, P. P.; Cao, Y.; Mao, C. J.; Jin, B. K.; Zhu, J. J. TiO_2/g-C_3N_4/CdS Nanocomposite-Based Photoelectrochemical Biosensor for Ultrasensitive Evaluation of T4 Polynucleotide Kinase Activity *Anal. Chem.* 2019, *91*, 1563-1570.

6. Sun, Y. Y.; Tian, W. M.; Liu, C. H.; Gao, K. J.; Li, Z. P. A Novel Restriction Endonuclease GlaI for Rapid and Highly Sensitive Detection of DNA Methylation Coupled with Isothermal Exponential Amplification Reaction *Chem. Sci.* 2018, *9*, 1344-1351.

7. Liu, Y. L.; Zeng, H. M.; Chai, Y. Q.; Yuan, R.; Liu, H. Y. Ti_3C_2/$BiVO_4$ Schottky Junction as a Signal Indicator for Ultrasensitive Photoelectrochemical Detection of $VEGF_{165}$ *Chem. Commun.* 2019, *55*, 13729-13732.

8. Zhang, Y. H.; Li, M. J.; Wang, H. J.; Yuan, R.; Wei, S. P. Supersensitive Photoelectrochemical Aptasensor Based on Br,N-Codoped TiO_2 Sensitized by Quantum Dots *Anal. Chem.* 2019, *91*, 10864-10869.

9. Wen, S. P.; Su, Y.; Dai, C. X.; Jia, J. R.; Fan G. C.; Jiang, L. P.; Song, R. B.; Zhu, J. J. Plasmon Coupling-Enhanced Raman Sensing Platform Integrated with Exonuclease-Assisted Target Recycling Amplification for Ultrasensitive and Selective Detection of microRNA-21 *Anal. Chem.* 2019, *91*, 12298-12306.

10. Yu, Y. j.; Ma, L.; Li, L. D.; Deng, Y. N.; Xu, L. D.; Liu, H.; Xiao, L. H.; Su, X. Digestion of Dynamic Substrate by Exonuclease Reveals High Single-Mismatch Selectivity *Anal. Chem.* 2018, *90*, 13655-13662.

11. Yin, B. C.; Liu, Y. Q.; Ye, B. C. One-Step, Multiplexed Fluorescence Detection of microRNAs Based on Duplex-Specific Nuclease Signal Amplification *J. Am. Chem. Soc.* 2012, *134*, 5064-5067.

12. Xu, Q. F.; Ma, F.; Huang, S. Q.; Tang, B.; Zhang, C. Y. Nucleic Acid Amplification-Free Bioluminescent Detection of MicroRNAs with High Sensitivity and Accuracy Based on Controlled Target Degradation *Anal. Chem.* 2017, *89*, 7077-7083.

13. Li, M. J.; Xiong, C.; Zheng, Y. N.; Liang, W. B.; Yuan, R.; Chai, Y. Q. Ultrasensitive Photoelectrochemical Biosensor Based on DNA Tetrahedron as Nanocarrier for Efficient Immobilization of CdTe QDs-Methylene Blue as Signal Probe with Near-Zero Background Noise *Anal. Chem.* 2018, *90*, 8211-8216.

14. Hou, T.; Xu, N. N.; Wang, W. X.; Ge, L.; Li, F. Truly Immobilization-Free Diffusivity-Mediated Photoelectrochemical Biosensing Strategy for Facile and Highly Sensitive MicroRNA Assay *Anal. Chem.* 2018, *90*, 9591-9597.

15. Zheng, Y. N.; Liang, W. B.; Xiong, C. Y.; Yuan, Y. L.; Chai, Y. Q.; Yuan, R. Self-Enhanced Ultrasensitive Photoelectrochemical Biosensor Based on Nanocapsule Packaging Both Donor-Acceptor-Type Photoactive Material and Its Sensitizer *Anal.*

Chem. 2016, *88*, 8698-8705.

16. Gao, X. S.; Cai, Q. Q.; Li, H. K.; Jie, G. F. Supersandwich Nanowire/Quantum Dots Sensitization Structure-Based Photoelectrochemical "Signal-On" Platform for Ultrasensitive Detection of Thrombin *Anal. Chem.* 2020, *92*, 6734-6740.

17. Zeng, R. J.; Luo, Z. B.; Su, L. S.; Zhang, L. J.; Tang, D. P.; Niessner, R.; Knopp, D. Palindromic Molecular Beacon Based Z-Scheme BiOCl-Au-CdS Photoelectrochemical Biodetection *Anal. Chem.* 2019, *91*, 2447-2454.

18. Deng, H. M.; Zhu, M. H.; Huang, L. J.; Chai, Y. Q.; Liu, X. R.; Yuan, R.; Yuan, Y. L. Novel D-A-D-Type Supramolecular Aggregates with High Photoelectric Activity for Construction of Ultrasensitive Photoelectrochemical Biosensor *Anal. Chem.* 2019, *91*, 12468-12475.

19. Zhang, D. Y.; Seelig, G. Dynamic DNA Nanotechnology Using Strand-Displacement Reactions *Nat. Chem.* 2011, *3*, 103-113.

20. Hong, T. T.; Yuan, Y. S.; Wang, T. L.; Ma, J. W.; Xiao, Q. Y.; Hua, L.; Xia, Y.; Zhou, X. Selective Detection of N6-Methyladenine in DNA via Metal Ion-Mediated Replication and Rolling Circle Amplification *Chem. Sci.* 2017, *8*, 200-205.

21. Zhang, N.; Shi, X. M.; Guo, H. Q.; Zhao, X. Z.; Zhao, W. W.; Xu, J. J.; Chen, H. Y. Gold Nanoparticle Couples with Entropy-Driven Toehold-Mediated DNA Strand Displacement Reaction on Magnetic Beads: Toward Ultrasensitive Energy-

Transfer-Based Photoelectrochemical Detection of miRNA-141 in Real Blood Sample *Anal. Chem.* 2018, *90*, 11892-11898.

22. Du, Y. C.; Cui, Y. X.; Li, X. Y.; Sun, G. Y.; Zhang, Y. P.; Tang, A. N.; Kim, K.; Kong, D. M. Terminal Deoxynucleotidyl Transferase and T7 Exonuclease-Aided Amplification Strategy for Ultrasensitive Detection of Uracil-DNA Glycosylase *Anal. Chem.* 2018, *90*, 8629-8634.

23. Miao, P.; Zhang, T.; Xu, J. H.; Tang, Y. G. Electrochemical Detection of miRNA Combining T7 Exonuclease-Assisted Cascade Signal Amplification and DNA-Templated Copper Nanoparticles *Anal. Chem.* 2018, *90*, 11154-11160.

24. Gao, H.; Zhang, J. F.; Liu, Y.; Tu, W. W.; Wei, T. X.; Dai, Z. H. Triple-Helix Molecular Switch Electrochemiluminescence Nanoamplifier Based on a S-Doped Lu_2O_3/Ag_2S Pair for Sensitive MicroRNA Detection *Anal. Chem.* 2019, *91*, 12038-12045.

25. Liu, R.; Hu, J. Y.; Chen, Y. X.; Jiang, M.; Lv, Y. Label-Free Nuclease Assay with Long-Term Stability *Anal. Chem.* 2019, *91*, 8691-8696.

26. Zhou, Y.; Zhang, Y.; Lin, M.; Long, J.; Zhang, Z.; Lin, H.; Wu, J. C.; Wang, X. Monolayered Bi_2WO_6 nanosheets mimicking heterojunction interface with open surfaces for photocatalysis *Nat. Commun.* 2015, *6*, 8340.

27. Tang, J.; Zou, Z.; Ye, J. Photocatalytic Decomposition of Organic Contaminants

by Bi2WO6 Under Visible Light Irradiation *Catal. Lett.* 2004, *92*, 53-56.

28. Tian, J.; Sang, Y.; Yu, G.; Jiang, H.; Mu, X.; Liu, H. A Bi_2WO_6-Based Hybrid Photocatalyst with Broad Spectrum Photocatalytic Properties under UV, Visible, and Near-Infrared Irradiation *Adv. Mater.* 2013, *25*, 5075-5080.

29. Sheng, J. Y.; Li, X. J.; Xu, Y. M. Generation of H_2O_2 and OH Radicals on Bi_2WO_6 for Phenol Degradation under Visible Light *ACS Catal.* 2014, *4*, 732-737.

30. Zang, Y.; Gong, L. J.; Mei, L. Q.; Gu, Z. J.; Wang, Q. Bi_2WO_6 Semiconductor Nanoplates for Tumor Radiosensitization through High-Z Effects and Radiocatalysis *ACS Appl. Mater. Interfaces* 2019, *11*, 18942-18952.

31. Liang, L.; Lei, F. C.; Gao, S.; Sun, Y. F.; Jiao, X. C.; Wu, J.; Qamar, S.; Xie, Y. Single Unit Cell Bismuth Tungstate Layers Realizing Robust Solar CO_2 Reduction to Methanol *Angew. Chem. Int. Ed.* 2015, *54*, 13971-13974.

32. Zhou, Y. G.; Zhang, Y. F.; Lin, M. S.; Long, J. L.; Zhang, Z. Z.; Lin, H. X.; Wu, J. C. S.; Wang, X. X. Monolayered Bi_2WO_6 nanosheets mimicking heterojunction interface with open surfaces for photocatalysis *Nat. Commun.* 2015, *6*, 8340.

33. Yuan, L.; Weng, B.; Colmenares, J. C.; Sun, Y. G.; Xu, Y. J. Multichannel Charge Transfer and Mechanistic Insight in Metal Decorated 2D-2D Bi_2WO_6-TiO_2 Cascade with Enhanced Photocatalytic Performance *Small* 2017, *13*, 1702253.

34. Dong, G. J.; Zhang, Y. J.; Bi, Y. P. The Synergistic Effect of Bi_2WO_6 Nanoplates

and Co_3O_4 Cocatalysts for Enhanced Photoelectrochemical Properties *J. Mater. Chem. A* 2017, *5*, 20594-20597.

35. Yang, Z.; Huang, L.; Xie, Y.; Lin, Z.; Fan, Y.; Liu, D.; Chen, L.; Zhang, Z.; Wang, X. Controllable Synthesis of Bi2WO6 Nanoplate Self-Assembled Hierarchical Erythrocyte Microspheres Via a One-Pot Hydrothermal Reaction with Enhanced Visible Light Photocatalytic Activity. *Appl. Surf. Sci.* 2017, *403*, 326-334.

36. Nithya, V. D.; Selvan, R. K.; Kalpana, D.; Vasylechko, L.; Sanjeeviraja, C. Synthesis of Bi_2WO_6 Nanoparticles and Its Electrochemical Properties in Different Electrolytes for Pseudocapacitor Electrodes. *Electrochim. Acta* 2013, *109*, 720-731.

37. Nithya, V. D.; Selvan, R. K.; Vasylechko, L.; Sanjeeviraja, C. Effect of Carbon Coating on the Electrochemical Properties of Bi_2WO_6 Nanoparticles by PVP-Assisted Sonochemical Method. *J. Appl. Electrochem.* 2015, *45*, 473-485.

38. Fu, H.; Pan, C.; Zhang, L.; Zhu, Y. Synthesis, Characterization and Photocatalytic Properties of Nanosized Bi_2WO_6, $PbWO_4$ and $ZnWO_4$ Catalysts. *Mater. Res. Bull.* 2007, *42*, 696-706.

39. Frost, R. L.; Duong, L.; Weier, M. Raman Microscopy of Selected Tungstate Minerals *Spectrochim. Acta A* 2004, *60*, 1853-1859.

40. Kaur, A.; Kansal, S. K. Bi_2WO_6 Nanocuboids: An Efficient Visible Light Active Photocatalyst for the Degradation of Levofloxacin Drug in Aqueous Phase *Chem.*

Eng. J. 2016, *302*, 194-203.

41. Zhang, K.; Dong, H. F.; Dai, W. H.; Meng, X. D.; Lu, H. T.; Wu, T. T.; Zhang, X. J. Fabricating Pt/Sn-In_2O_3 Nanoflower with Advanced Oxygen Reduction Reaction Performance for High-Sensitivity MicroRNA Electrochemical Detection *Anal. Chem.* 2017, *89*, 648−655.

42. Peng, X.; Wen, Z. B.; Yang, P.; Chai, Y. Q.; Liang, W. B.; Yuan, R. Biomimetic 3D DNA Nanomachine via Free DNA Walker Movement on Lipid Bilayers Supported by Hard SiO_2@CdTe Nanoparticles for Ultrasensitive MicroRNA Detection *Anal. Chem.* 2019, *91*, 14920-14926.

43. Cheng, Y. Y.; Xie, Y. F.; Li, C. M.; Li, Y. F.; Huang, C. Z. Förster Resonance Energy Transfer-Based Soft Nanoballs for Specific and Amplified Detection of MicroRNAs *Anal. Chem.* 2019, *91*, 11023-11029.

44. Lu, L. P.; Wang, J. X.; Miao, W. J.; Wang, X. Y.; Guo, G. S. Electrogenerated Chemiluminescence Biosensor with a Tripod Probe for the Highly Sensitive Detection of MicroRNA *Anal. Chem.* 2019, *91*, 1452-1459.

45. Li, C. X.; Lu, W. S.; Zhou, X. M.; Pang, M. M.; Luo, X. L. Visible-Light Driven Photoelectrochemical Platform Based on the Cyclometalated Iridium(III) Complex with Coumarin 6 for Detection of MicroRNA *Anal. Chem.* 2018, *90*, 14239-14246.

46. Zhang, N.; Shi, X. M.; Guo, H. Q.; Zhao, X. Z.; Zhao, W. W.; Xu, J. J.; Chen, H.

Y. Gold Nanoparticle Couples with Entropy-Driven Toehold-Mediated DNA Strand Displacement Reaction on Magnetic Beads: Toward Ultrasensitive Energy-Transfer-Based Photoelectrochemical Detection of miRNA-141 in Real Blood Sample *Anal. Chem.* 2018, *90*, 11892-11898.

For TOC Only

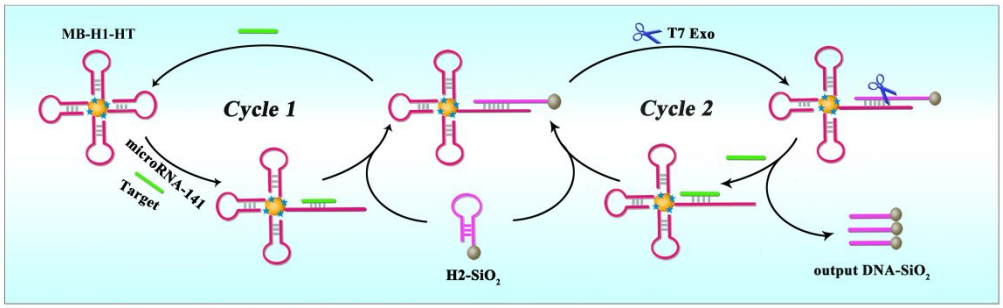
MB-H1-HT
Cycle 1
microRNA-141
Target
H2-SiO2
T7 Exo
Cycle 2
output DNA-SiO2